Monthly Notices
of the
ROYAL ASTRONOMICAL SOCIETY

Mon. Not. R. Astron. Soc. **408,** 2149–2162 (2010) doi:10.1111/j.1365-2966.2010.17055.x

δ Sct-type pulsations in eclipsing binary systems: Y Cam

E. Rodríguez,[1⋆] J. M. García,[2] V. Costa,[1] P. Lampens,[3] P. van Cauteren,[4] D. E. Mkrtichian,[5] E. C. Olson,[6] P. J. Amado,[1] J. Daszyńska-Daszkiewicz,[7] V. Turcu,[8] S.-L. Kim,[9] A. Y. Zhou,[10] M. J. López-González,[1] A. Rolland,[1] D. Díaz-Fraile,[1] M. A. Wood,[11] E. Hintz,[12] A. Pop,[8] D. Moldovan,[8] P. B. Etzel,[13] V. Casanova,[1] A. Sota,[1] F. J. Aceituno[1] and D.-J. Lee[9]

[1]*Instituto de Astrofísica de Andalucía, CSIC, PO Box 3004, E-18080 Granada, Spain*
[2]*Departamento de Física Aplicada, EUITI, Universidad Politécnica de Madrid, Ronda de Valencia 3, E-28012 Madrid, Spain*
[3]*Koninklijke Sterrenwacht van België, Ringlaan 3, 1180 Brussels, Belgium*
[4]*Beersel Hills Observatory, Laarheidestraat 166, 1650 Beersel, Belgium*
[5]*Crimean Astrophysical Observatory, Nauchny, OCrimea, 98409, Ukraine*
[6]*Astronomy Department, University of Illinois, 1002 W. Green St., Urbana, IL 61801, USA*
[7]*Instytut Astronomiczny, Uniwersytet Wroclawski, ul. Kopernika 11, 51-622 Wroclaw, Poland*
[8]*Astronomical Institute of the Romanian Academy, Astronomical Observatory Cluj-Napoca, Str. Cireşilor 19, 400487 Cluj-Napoca, Romania*
[9]*Korea Astronomy and Space Science Institute, Daejeon 305-348, Korea*
[10]*National Astronomical Observatories, Chinese Academy of Sciences, Beijing 100012, China*
[11]*Department of Physics & Space Sciences and SARA Observatory, Florida Institute of Technology, Melbourne, FL 32901, USA*
[12]*Department of Physics and Astronomy, Brigham Young University, Provo, UT 84602, USA*
[13]*Department of Astronomy, San Diego State University, San Diego, CA 92182, USA*

Accepted 2010 May 19. Received 2010 May 18; in original form 2010 February 6

ABSTRACT

We present the results of a three-continent multisite photometric campaign carried out on the Algol-type eclipsing binary system Y Cam, in which the primary component is a multiperiodic δ Sct-type pulsator. The observations consist of 86 nights and more than 450 h of useful data collected mainly during the Northern winter 2002–2003. This means that this is the most extensive time series for such kind of systems obtained so far. These observations were collected mostly in the Johnson V filter, but they also include, for the first time, nearly complete binary light curves in simultaneous Strömgren *uvby* filters together with a few Crawford Hβ data obtained around the orbital phase of the first quadrature. A detailed photometric analysis is presented for both binarity and pulsation. The results indicate a semidetached system with the secondary filling its Roche lobe. No significant contribution from a third body is found. The residuals from the computed binary solution were then used to investigate the pulsational content of the primary component. The frequency analysis of the out-of-primary-eclipse data leads to a set of eight significant and independent pulsational peaks in a well-defined region of the frequency domain. This means that this is the largest set of excited modes discovered so far in the pulsating component of such kind of systems. The possibility of aliasing problems during the present run or short-term time-scale amplitude variations in some of them was investigated with null results. Indeed the results indicate that f_1 and f_3 form a frequency doublet with a beat period of $P_{\rm beat} = 17.065$ d. Our results confirm the frequencies already detected by earlier authors and show the presence of some additional significant peaks. The observed amplitudes during the present run are also consistent with those derived from older data sets. We perform a preliminary mode identification for most of the frequencies on the basis of the collected multicolour photometry, the observed frequency spacings and the mode visibility in eclipsing binaries.

Key words: techniques: photometric – binaries: eclipsing – stars: individual: Y Cam – stars: oscillations – stars: variables: δ Scuti.

⋆E-mail: eloy@iaa.es

1 INTRODUCTION

In January 2000 (Rodríguez & Breger 2001), only about one-tenth of δ Sct pulsators were known as members of eclipsing binary systems, and only half of them were components of semidetached Algol-type binaries, the so-called oEA stars (oscillating EA stars, Mkrtichian et al. 2004). The oEA stars are 'mass-accreting main-sequence A/F-type components in semidetached Algol-type eclipsing binary systems showing δ Sct-like pulsation'. The number of known oEA stars has been largely increased during the last few years until more than 20 members (Lampens et al. 2008; Mkrtichian et al. 2007a, and references therein) and several tens of candidates have also been proposed (Soydugan et al. 2006). The first example of high-amplitude δ Sct star as a member of the oEA class was recently proposed (Christiansen et al. 2007), as is also the case with the first SX Phe pulsator (among the blue stragglers of the metal-rich globular cluster M71, Jeon et al. 2006) and the first γ Dor candidate (one component of the close binary system VZ CVn, Ibanoglu et al. 2007). However, only a few oEA stars can be considered as well-studied examples concerning their frequency content, some of them have been studied through multisite photometric campaigns: RZ Cas (Rodríguez et al. 2004a), AB Cas (Rodríguez et al. 2004b), AS Eri (Mkrtichian et al. 2004), AB Per (Kim et al. 2003; Kim, Lee & Lee 2006), IV Cas (Kim et al. 2007) and CT Her (Lampens et al. 2008, 2010).

The oEA stars are very attractive targets for asteroseismology because of the great variety in their pulsational behaviour concerning the frequency content, nature of the modes and long-term pulsational behaviour. One clear example is RZ Cas (Rodríguez et al. 2004a; Lehmann & Mkrtichian 2004, 2008, Mkrtichian et al., in preparation) where evident changes in the number and amplitude of the excited modes, together with strong pulsational modulations, are found with time-scales of years. Moreover, in the oEA stars there is coexistence of pulsations, binarity (including tidal effects) and other effects such as mass-transfer episodes that can affect the pulsation properties, which can be simultaneously studied within a unique framework. In the case of RZ Cas, abrupt changes in the orbital period were detected during the years 2000–2001 which seem to be correlated to abrupt changes in the pulsational pattern of the primary component. They are suggested to be originally caused by magnetic activity of the cool component producing episodes of more intense mass-transfer to the gainer. The higher mass-transfer in 2001 resulted in a dense circumstellar gas envelope that suppressed the periodic spatial filter effect (see Gamarova et al. 2003) during primary eclipses. A detailed analysis of the amplification due to the periodic spatial filter effect and its use for the identification of the pulsation modes in the primary component of RZ Cas is in preparation (Mkrtichian et al., in preparation). The identification of pulsational modes using the Spatial Filtration method (Gamarova et al. 2003) during the primary eclipses was already used for RZ Cas with successful results (Rodríguez et al. 2004a), for photometry carried out in 1999.

In the present work we deal with the Algol-type eclipsing binary system Y Cam (A9IV+K1IV, $V = 10.5$ mag, Rodríguez & Breger 2001) discovered by Baker (1937), where the primary component is a multiperiodic δ Sct-type pulsator. The orbital period is $P_{\rm orb} = 3.3057$ d (Kim et al. 2002) with primary and secondary eclipse depths of $\Delta V \sim 1.7$ and 0.1 mag, respectively. The main pulsation period of the primary is $P_{\rm pul} = 0.0665$ d with a peak-to-peak amplitude of $\Delta \sim 0.04$ mag . The pulsational behaviour was discovered photometrically in filters B and V by Broglia (1973), and confirmed by the analysis of these observations by Broglia & Marin (1974). New BV photometric data were obtained and analysed by Broglia & Conconi (1984) which revealed a non-radial nature and multiperiodic behaviour for the pulsating component of Y Cam, with two close excited modes and probably amplitude changes. This was also confirmed by a new and larger photometric V data set obtained by Kim et al. (2002). In this case, four significant peaks were found.

Here we present the results of a multisite and multicolour photometric campaign carried out on Y Cam with the main aim of performing a detailed study from both binary and pulsational point of view. The observations and data reduction are described in Sections 2 and 3. In Sections 4 and 5, we present the analysis and results for binarity and pulsation. Section 6 summarizes the main conclusions.

2 OBSERVATIONS

The data were collected between October, 2002, and April, 2003, at eight observatories distributed in Europe, Asia and America. Multicolour photometry was additionally secured on one night of February, 2004, at Sierra Nevada Observatory (SNO) with the aim of covering the secondary minimum of Y Cam. This was successfully done for the three *vby* filters, but technical problems with the ultraviolet photomultiplier rendered the data collected in *u* filter useless. Table 1 lists the observatories and instrumentation used in this work together with the journal of the collected observations. At SNO, two different telescopes (90 and 150 cm) and instruments (multichannel photometer and CCD camera) were used. In total, photometric data on 86 nights and 464 h of useful observations were acquired. This means the most extensive time series obtained so far for such kind of systems. Moreover, some additional observations were tried with the 75-cm Vienna Automatic Photoelectric Telescope (APT) in Arizona, but pointing problems of this telescope at high declinations made these data useless.

Most of the observations were collected using CCD cameras and the Johnson V filter in order to get a data set as homogeneous as possible to perform a reliable frequency analysis. Additionally, at Mount Laguna Observatory (MLO) a single photomultiplier with the V filter was used. Simultaneous multicolour Strömgren *uvby* photometry was also carried out using the six-channel *uvbyβ* photometer attached to the 90-cm telescope at SNO (hereafter SNO/T90) with the aim to perform a detailed study of the binary light curve and to investigate the consistency of the detected peaks through different filters. With purposes of calibration, a few Crawford Hβ data were also obtained at binary phase around 0.25 using the same telescope.

3 DATA REDUCTION

All CCD measurements were obtained by the method of synthetic aperture photometry. Each CCD frame was corrected in a standard way for dark, bias and flat-field. The nearby star SAO 6274 ($V = 10.3$ mag , ST = A5), of similar brightness and spectral type as Y Cam, located in the same frame as the variable, was selected as the main comparison star in order to derive the corresponding magnitude differences. It was also selected by earlier authors in different works (Broglia & Conconi 1984; Kim et al. 2002). A number of additional check stars were also selected within the frame of the variable testing for possible variability, with unsuccessful results. The integration times, typically 10–100 s, were adopted according to the instrumentation used in each case. This provided typical photometric uncertainties for each individual measurement of

Table 1. Participating sites and instrumentation. Observatory codes: SNO, Sierra Nevada Observatory; BHO, Beersel Hills Observatory; CNAO, Cluj-Napoca Astronomical Observatory; SOAO, Sobaeksan Optical Astronomical Observatory; BAO Beijing Astronomical Observatory; KPNO, Kitt Peak National Observatory; OPO, Orson Pratt Observatory; MLO, Mount Laguna Observatory. Detectors: PMT, single photomultiplier; Simul, simultaneous spectrograph *uvby* photometer.

Obs	Location	Telescope	Detector	Filters	Nights	Hours
SNO/T90	Granada (Spain)	90 cm	Simul	*uvby*	24	128
SNO/T150	Granada (Spain)	150 cm	CCD	V	9	57
BHO	Beersel (Belgium)	40 cm	CCD	V	21	106
CNAO	Cluj-Napoca (Romania)	40 cm	CCD	V	9	40
SOAO	Sobaeksan (Korea)	61 cm	CCD	V	5	26
BAO	Xing Long, Beijing (China)	85 cm	CCD	V	3	27
KPNO	Kitt Peak, Arizona (USA)	90 cm	CCD	V	4	23
OPO	Provo, Utah (USA)	40 cm	CCD	V	4	19
MLO	Mount Laguna, California (USA)	100 cm	PMT	V	7	38

Y Cam ranging between 0.002 and 0.03 mag depending on each participating site. Nevertheless, in time series with the shortest integration times, the data were binned every certain number of measurements in order to diminish the dispersion of the data points. This was also made with the aim to adapt the number of observing points from each contribution to its number of collected observing hours taking as reference the rate from the SNO/T90 contribution, that is, about 15 points/hour, as shown below. In this way, the weights of each contribution for the frequency analysis performed in Section 5 are, to a first approximation, related directly to their number of observing hours.

In the case of observations obtained with photomultipliers (MLO and SNO/T90), similar sequential observing programmes were followed with one main comparison star C1 = HD 59641 and two check stars C2 = HD 58710 and C3 = HD 60404. After a few nights, C3 was revealed as a new multiperiodic low-amplitude δ Sct variable with a main period of about 1 h (Fig. 1), but no sign of periodicity was found for C1 nor for C2 (Fig. 2). Then, C3 was removed from the observational sequence which typically continued as C1, C2, Var with sky measurements every two or three cycles. Concerning the SNO observations, the integration times were of 90 s for Var, 40 s for C1 and C2 and 20 s for the sky. This means one observational point of Y Cam about every 4 min and an internal error per observation better than 0.004 mag in filters *vby* or 0.009 mag in the *u* filter. The extinction corrections were based on nightly coefficients determined from the main comparison star. Then, magnitude differences of each object relative to C1 were calculated by means of linear interpolation.

The multicolour SNO/T90 data were transformed into the standard *uvbyβ* system following the procedure described in Rodríguez et al. (2003), using C1 and C2 as zero-points for *uvby* photometry and C3 and the nearby star HD 66170 as zero-points for Hβ photometry. Thus, the resulting *y* are similar to the V ones into the standard Johnson system. Derived *uvbyβ* indices for Y Cam (at first quadrature) and the two main comparison stars C1 and C2 are listed in Table 2 together with some relevant catalogue information on these objects. The derived indices for C1 and C2 are in very good agreement with those found in the bibliography (Olsen, private communication; Hauck & Mermilliod 1998).

These indices together with the catalogued ones for C3 = HD 60404 ($b-y = 0.174$ mag, $m_1 = 0.218$ mag, $c_1 = 0.757$ mag and $\beta = 2.766$ mag) can be used to locate the comparison stars in the HR diagram using suitable calibrations available in the literature for *uvbyβ* photometry (Rodríguez et al. 2001). Fig. 3 shows the locations of Y Cam (primary component only using the parameters derived in Section 4) and the comparison stars. C3 is well inside the instability region of the δ Sct-type pulsators, but slightly overabundant in metals [[Me/H] = 0.4(±0.1)].

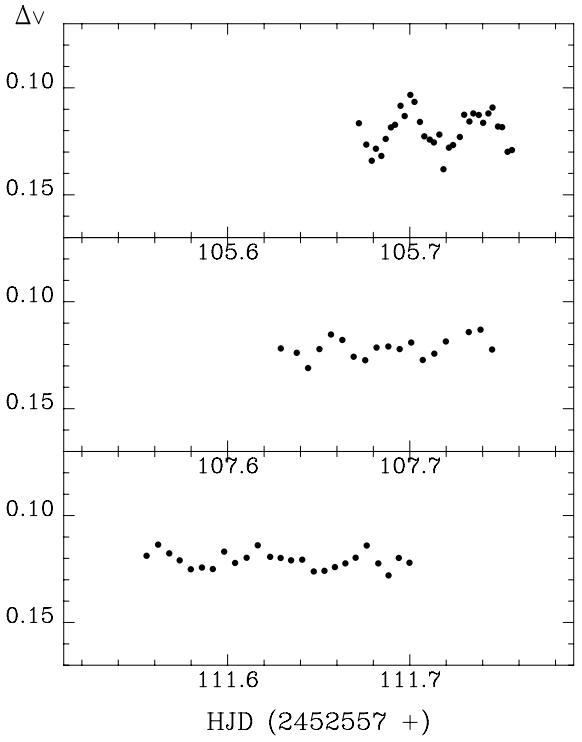

Figure 1. Observed light variations of the new δ Sct star C3 = HD 60404 in the Strömgren *v* band. The *y*-axis is magnitude differences C3 – C1.

4 BINARITY

4.1 Light curves

Twelve times primary minima were determined from the present data, using the method described in Rodríguez et al. (1990). They are listed in Table 3. In the case of observations collected at SNO, the four filters *uvby* were used for averaging. The secondary eclipse was also covered a few times in the V filter, but the distortions in the binary light curve caused by the pulsational behaviour are too large when trying to obtain reliable times of minimum directly from the observations. As mentioned in Section 1, the secondary

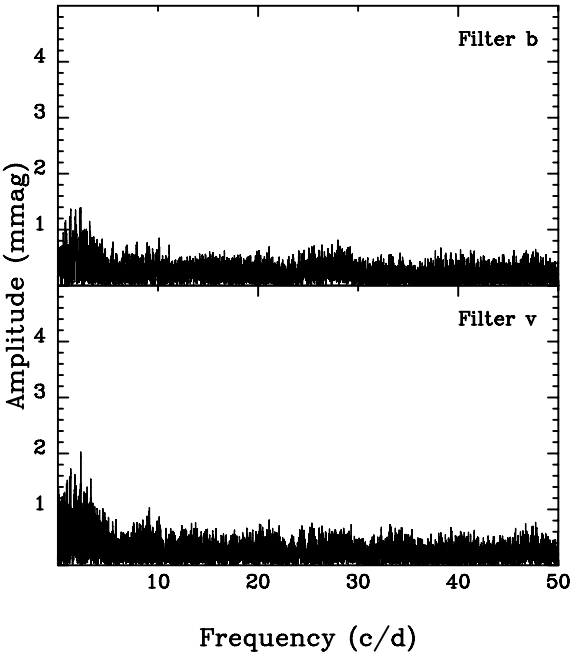

Figure 2. Amplitude spectra of C2 = HD 58710 minus C1 = HD 59641 in the *b* and *v* bands.

Table 2. Data for Y Cam (photometry at phase 0.25) and the two main comparison stars used for the multicolour *uvbyβ* observations.

	Variable	Comp. 1	Comp. 2
HD no.		59641	58710
BD no.	+76°00286	+76°00284	+74°00327
SAO no.		6258	6234
HIP no.	37440	37252	36805
α_{2000}	$07^h41^m11\overset{s}{.}0$	$07^h39^m02\overset{s}{.}5$	$07^h34^m10\overset{s}{.}9$
δ_{2000}	+76°04′26″	+75°47′10″	+74°21′35″
l	139°	139°	141°
b	29°	29°	29°
ST	A9IV+K1IV	F5	F2
V	10.509(8) mag	7.748(6) mag	8.049(6) mag
b-y	0.181(7) mag	0.316(5) mag	0.271(5) mag
m_1	0.158(8) mag	0.152(5) mag	0.153(5) mag
c_1	0.962(15) mag	0.432(10) mag	0.538(10) mag
β	2.777(15) mag	2.635(5) mag	2672(8) mag

minimum was also observed one time in the *uvby* bands, but the data obtained in *u* filter were useless.

In order to phase our *uvby* data, a linear ephemeris with initial epoch $T_0 = 2452\,710.4649$ d (one of our present *uvby* times of primary minimum) and orbital period $P_{\rm orb} = 3.305\,744\,92$ d (Kim et al. 2002) was used. Fig. 4 shows the resulting *v* light curve together with the corresponding colour index variations along the orbital cycle. Nearly all orbital phases were covered at least once, except a small interval centred at secondary minimum and filter *u*. As shown in the figure, the colour index variations reflect the temperature and luminosity differences of the two components. The observed primary eclipse depths corresponding to the various passbands were $\Delta u = 1.96$ mag, $\Delta v = 2.00$ mag, $\Delta b = 1.86$ mag and $\Delta y = 1.72$ mag and $\Delta u \sim 0.04$ mag, $\Delta v = 0.05$ mag, $\Delta b = 0.07$ mag and $\Delta y = 0.09$ mag for the secondary eclipses. Contrary to that occurring in other cases as RZ Cas (Rodríguez et al. 2004a), significant distortions (e.g. reflection and ellipticity) or asymmetries

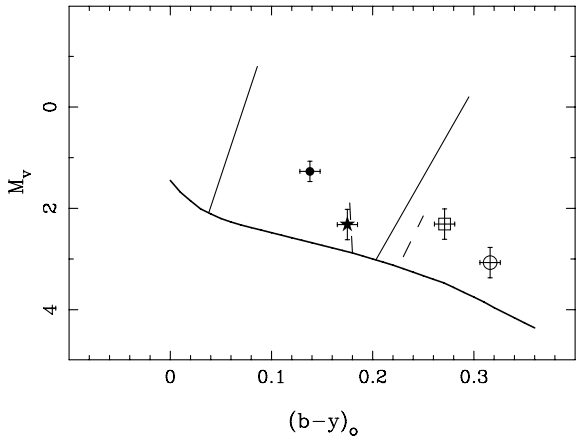

Figure 3. Location of Y Cam (filled circle), C1 = HD 59641 (open circle), C2 = HD 58710 (open square) and C3 = HD 60404 (star) in the HR diagram. The observational edges of the δ Sct instability region (solid lines) are from Rodríguez & Breger (2001) and those for the γ Dor region are from Handler & Shobbrook (2002).

Table 3. Times of primary minima collected in this work.

HJD 2450000.+ (d)	Error (d)	Filter
2558.3989	0.0005	V
2601.3732	0.0010	V
2624.5143	0.0010	V
2660.8780	0.0010	V
2677.4052	0.0005	V
2680.7070	0.0005	V
2687.3261	0.0005	V
2690.6303	0.0005	V
2697.2412	0.0005	V
2700.5467	0.0010	*uvby*
2710.4649	0.0010	*uvby*
2733.6041	0.0010	*uvby*

due to the Rossiter–McLaughlin effect (occurring at the phase of primary eclipse) are not observed in the light curves of Y Cam. The pulsation cycles only seem to be shown, although the relative large amplitude of the pulsations might mask any other small feature in Fig. 4.

4.2 Photometric analysis

Light variations coming from binarity must be carefully subtracted in order to proceed to the study of the pulsational characteristics of the primary component. With this purpose, we used the 2003 version of Wilson–Devinney (WD) code (Wilson & Devinney 1971; Wilson 1979, 1990; van Hamme & Wilson 2003; Wilson & van Hamme 2004). Magnitude differences at quadrature (phase 0.25) of 2.900 (u), 2.497 (v), 2.626 (b) and 2.761 (y) were used to obtain the normalized light for each observational point. The effective temperature $T_1 = 7500$ K adopted for the primary component was derived from our *uvbyβ* colour indices and the calibration by Moon & Dworetsky (1985). This value is consistent with the spectral type A9IV given by Breger (1979) for the primary component of Y Cam. Since the secondary eclipse is very shallow, the δ Sct-type pulsations introduce a large uncertainty in the timings of the secondary

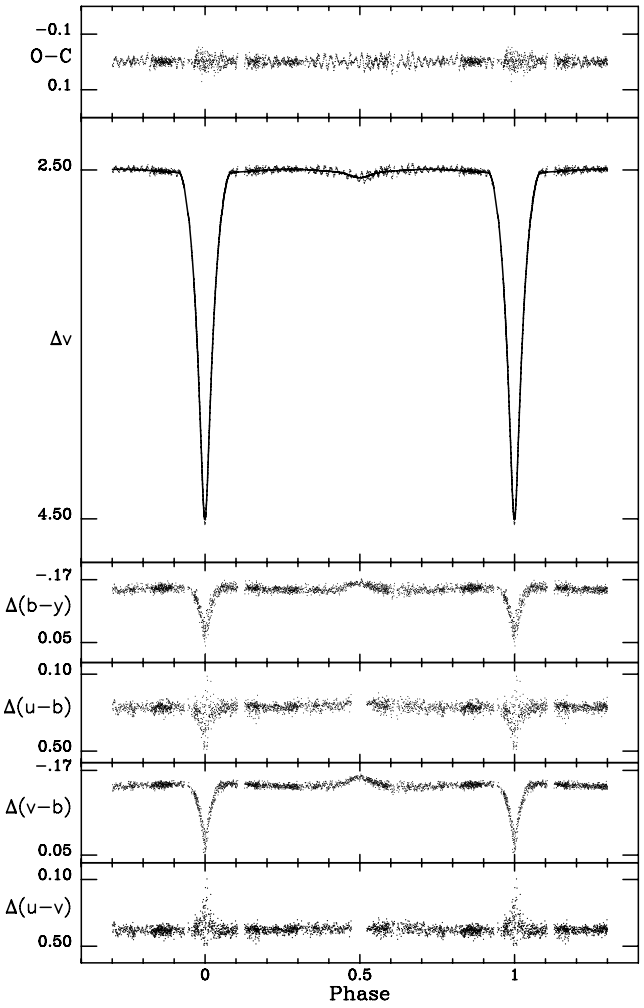

Figure 4. v light curve and colour index variations of Y Cam together with the synthetic v binary solution and residuals.

minimum. Nevertheless, the secondary eclipse is essentially centred at phase 0.5 and the light curve appears symmetrical. Hence, in absence of contrary evidences, we have considered a circular orbit ($e = 0.0$). Several other basic assumptions were made for solving the *uvby* light curves: linear limb-darkening coefficients for each band were taken from Díaz-Cordovés, Claret & Giménez (1995), theoretical values of the bolometric albedos ($A_1 = 1.0$ and $A_2 = 0.5$) and gravity-darkening exponents ($g_1 = 1.0$ and $g_2 = 0.32$) were adopted for the primary and secondary stars, corresponding to radiative and convective envelopes, respectively, in agreement with their final surface temperatures.

Based on the results of previous photometric analyses on the BV light curves (Broglia & Conconi 1984; Lee et al. 2002), suggesting a detached configuration, we tried formerly to solve the light curves in Mode 2, appropriate for detached systems. After several initial runs, we found incoherent results for the different bands and the tendency of the secondary component to exceed the size of the inner critical Roche lobe. Therefore Mode 5, corresponding to the secondary star filling its Roche lobe, was adopted for the subsequent analysis. Such semidetached configuration is, on the other hand, typical of Algol-type binaries like Y Cam. This is also in agreement with the results found by Mezzetti et al. (1980). Since no spectroscopic mass-ratio, q, is known, we carried out a grid search by solving the light curves with assumed q values in the range of 0.14–0.40 in steps of 0.02. The minimum value of the residuals is reached around $q = 0.24$ within a range of ± 0.004 where the residuals obtained are equally small for slight variations of the other parameters. The values of q obtained for the individual colours [0.245(u), 0.241 (v), 0.242 (b) and 0.240 (y)] are internally consistent. Hence a mean value $q = 0.241$ from *vby* filters was adopted along the subsequent analysis. Still, this value should be handled cautiously as pointed out by Rodríguez et al. (2004b) because it is implicitly related to the width and depth of the eclipses and both may be altered by pulsation.

After these former settings, the relevant parameters to be determined by the least-squares procedure were: the orbital inclination, i; the mean temperature of the secondary T_2; the potential, W_1; and the luminosity, L_1, of the primary star. The third light, l_3, was initially taken as zero. However, in view of the results of Broglia & Conconi (1984) and Mossakovskaya (1993), who argued in favour of the presence of a third body and, even of the possibility of a quadruple system, several runs were performed including l_3 alternately among the free parameters. No significant reduction in the residuals was however obtained when l_3 is different from zero. In fact the convergence leads to small values of l_3, only slightly bigger than its probable error bar. This is somehow expected, because the limit where the residuals are dominated by the δ Sct pulsations was already reached and they mask other fainter effects. We may conclude that, if present, the contribution of the l_3 is not bigger than about 0.01. Consequently, we adopt a null value in the final solution.

4.3 Results

Table 4 lists the elements obtained in our analysis for each colour separately. As commented before, the secondary minimum was not completely covered with the u filter and, hence, our results are not reliable in this band. Thus, although we performed the light-curve analysis for all four filters, this colour was excluded when calculating the mean final solution. Normalized luminosities for the primary and secondary components corresponding to the different wavebands, are calculated taking into account the mean geometrical elements given in the last column of Table 4. The light variations due to binarity are then calculated by means of the LC routine of WD from elements adopted in that table and subtracted from the observations in order to disclose the pulsational pattern. The theoretical light curve for filter v is shown in Fig. 4. The agreement between the observed (points) and the theoretical light curve (solid line) is quite good, with no systematic trends in the residuals. They uniquely seem to show the pulsational behaviour of the hotter component. The elements obtained in the present work differ from those of Broglia & Conconi (1984), mainly due to the adoption in their analysis of a value of the mass ratio $q = 0.35$ which is not confirmed by our study. However, our results are basically coincident with those provided by Lee et al. (2002) for Mode 5 and $l_3 = 0.0$.

Based on our determination of the geometrical elements, we can make a rough estimation of the absolute dimensions of Y Cam. The mass of the primary and secondary component stars can be calculated from our photometric mass ratio value $q = m_2/m_1 = 0.241$ and the mass function $f(m) = 0.015\,M_\odot$ (Struve et al. 1950), although the latter is poorly determined according to the remarks in Batten, Fletcher & MacCarthy (1989). Using the well-known relations for binary systems (see, e.g., Mezzetti et al. 1980) the masses, radii and luminosities for the individual components can be estimated. The results are listed in Table 5. An uncertainty of 20 per cent in the determination of the mass function $f(m)$ was

Table 4. WD solutions for Y Cam.

Parameter	*v*	*b*	*y*	Adopted
i (°)	85.77	85.53	85.48	85.6(1)
T_1 (K)				7500
T_2 (K)	4260	4320	4280	4290(60)
Ω_1	4.3419	4.3515	4.3210	4.338(9)
Ω_2				2.332
Phase shift (10^{-5})	−50	−50	−40	−47(3)
q	0.240	0.242	0.241	0.241
L_1	0.966	0.950	0.922	
L_2	0.034	0.050	0.078	
l_3				0.0
e				0.0
x_1	0.67	0.64	0.56	
x_2	0.95	0.94	0.84	
g_1				1.0
g_2				0.32
A_1				1.0
A_2				0.5
Max. (mag)	2.497	2.626	2.761	
r_1 pole	0.2434	0.2429	0.2447	0.2437(9)
r_1 point	0.2473	0.2468	0.2486	0.2476(9)
r_1 side	0.2456	0.2451	0.2470	0.2459(9)
r_1 back	0.2468	0.2463	0.2481	0.2471(9)
r_2 pole				0.2456
r_2 point				0.3585
r_2 side				0.2556
r_2 back				0.2882
χ^2	0.388	0.319	0.336	
rms (mag)	0.013	0.012	0.013	
Nr obs = 2061				

Table 5. Individual components of Y Cam.

Parameter	Primary	Secondary
Mass ($M_\odot$)	1.7(3)	0.41(7)
Radius ($R_\odot$)	2.95(17)	3.07(18)
log $L/L_\odot$	1.39(6)	0.46(6)
M_{bol} (mag)	1.28(15)	3.60(15)

assumed. The location of the components in a mass–radius diagram shows that both stars are clearly evolved with respect to the ZAMS, as it was expected from their luminosity class (A9IV for the primary star and K3III for the evolved, Roche-lobe filling secondary).

5 PULSATION

5.1 Frequency analysis

After the binary solution was removed from the data, a Fourier analysis was performed on the residuals to investigate the pulsational behaviour of the primary component of Y Cam. To make the frequency analysis more reliable, the orbital phases around the primary eclipse (between 0.9 and 0.1) were eliminated. These parts of the light curves often contain irregularities produced by systematic errors in obtaining the magnitude differences, variable minus comparison star and/or from subtracting the binary solution because the pulsational variations are very small as compared to the large depth of the primary minima. If some irregularities occurring in this region are real, they should be connected with the pulsations. Nevertheless, some chaotic changes are also commonly expected, caused by density variations of the gas-stream and circumbinary envelope. Thus, only out-of-eclipse phases were considered in our frequency analysis.

Table 6. Individual out-of-eclipse contributions for the Fourier analysis. σ means residuals after extraction of the full solution of eight peaks listed in Table 7. Observatory codes are the same as in Table 1.

Obs	Nights	Hours	Points	σ (mmag)
SNO/T90	17	94	1503	6.7
SNO/T150	8	41	534	4.6
BHO	19	81	1018	7.3
CNAO	5	15	246	15.2
SOAO	4	20	320	10.2
BAO	2	16	215	13.2
KPNO	2	10	151	7.7
OPO	2	8	122	11.7
MLO	7	38	558	9.4

The study of the pulsational content has been carried out following the procedure described in Rodríguez et al. (1998), where Fourier and least-squares algorithms are combined in the same computation program package. This method is similar to that followed by the computation package PERIOD (PERIOD04) (Lenz & Breger 2005) and both produced identical results in our analysis. When a new peak is found as significant in the frequency domain, this and all the previously determined frequencies are simultaneously optimized and extracted from the data together with the corresponding amplitudes and phases that minimize the residuals. Thus, the method does not depend on successive pre-whitening of the data.

We stop the analysis when the new peaks suggested in the periodograms are not formally significant. Following Breger et al. (1993, 1999), a peak is considered as significant when the amplitude signal/noise (S/N) ratio is larger than 4.0 for independent frequencies or larger than 3.5 for harmonics or frequency combinations. Once all the significant peaks were removed from the periodograms, the noise level was calculated on the residuals. This was made by averaging the amplitudes of the residuals over 5 cd^{-1} boxes around each frequency under consideration.

The individual out-of-eclipse contributions are listed in Table 6. The full data set consists of 4667 measurements collected along 323 h of observations on 66 nights with a time span of 200 d from October, 2002 to April, 2003. This strongly reduces the power of the daily (1 cd^{-1}) alias from 78 per cent (when only the SNO contribution is considered) to about 40 per cent and allows us a better identification of the true peaks in the periodograms, as can be seen in Fig. 5. One observing night (collected in February, 2004) was removed from the SNO/T90 contribution because this is too far from the bulk of the campaign. The last column in Table 6 refers to the rms of the residual in each contribution after extracting the final solution listed in Table 7.

Previously, each individual contribution in Table 6 was investigated to avoid misinterpretations in our final results as due to errors coming from a particular subset. This was done with the aim to obtain a final data set as homogeneous as possible. This way, inaccurate points were eliminated, and each subset was moved to mean zero level, $\langle V \rangle = 0$.

In a first step, the SNO/T90 multicolour contribution was considered for frequency content. As usual, when *uvby* photometry is

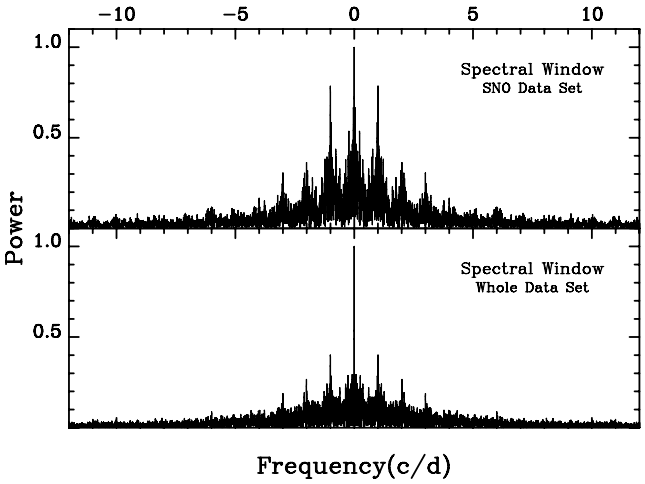

Figure 5. Spectral windows of Y Cam corresponding to the SNO and whole data sets.

Table 7. Results from frequency analysis applied to the whole data set. S/N are the amplitude signal-to-noise ratios. Sigma of the residuals is 8.5 mmag. Last column lists the corresponding pulsation constants.

Frequency (cd^{-1})	Amplitude (mmag)	S/N	Q (d)
	±0.18		
$f_1 = 15.046\,93$	8.22	17.3	0.0171
10			
$f_2 = 18.312\,16$	5.82	11.8	**0.0141**
15			
$f_3 = 14.988\,33$	4.72	9.9	0.0172
18			
$f_4 = 19.380\,45$	4.29	8.9	0.0133
19			
$f_5 = 17.707\,58$	3.66	7.4	**0.0145**
24			
$f_6 = 14.446\,80$	3.50	7.4	0.0178
24			
$f_7 = 14.841\,47$	3.38	7.1	0.0173
24			
$f_8 = 19.697\,67$	2.90	6.0	0.0131
30			

used to study the pulsational content of A–F stars, the data collected in *vb* bands are first analysed, since both amplitude and intensity in luminosity are larger in these two bands. Hence, the precisions in these filters are better and the results are more reliable. In fact, the results obtained in these two filters are in very good agreement with each other, and a set of six peaks are detected as significant, very close to those named $f_1, f_2, f_3, f_5{+}1, f_6$ and f_8 of Table 7. After removing these peaks, other terms are probably remaining in the residuals, but below the significance level.

For the sake of consistency in our results and to inspect our multicolour photometry in more depth, the *vby* data were aligned in a common filter *v* following the method described in Rodríguez et al. (2001). To simulate the amplitudes in *v* band, scale factors of 1.163 and 1.506 were applied to *b* and *y* data taking into account the amplitudes of the three main peaks previously found. Next, the *vby* measurements obtained at each instant were averaged with weights according to the precision in each filter. The corresponding weights were 1.0, 1.164 and 0.706 for *v*, *b* and *y*, respectively. When analysing this subset, we find a set of eight significant peaks very similar to those of Table 7. Finally, all the other contributions were scaled to the *v* filter of the SNO/T90 contribution in order to merge all the data in a unique data set.

5.1.1 Results

Table 7 lists the results when the frequency analysis is applied to the whole data set. A set of eight significant peaks is found. None of them corresponds to any combination of the others. All of them are in a well-defined region of the frequency domain, that is, between 14.4 and 19.7 cd^{-1}. Note that the error bars in Table 7 are only the formal error bars from the Fourier fitting, the result of the multiple-frequency non-linear least-squares fit to the data. They are very similar to the error bars for frequencies, amplitudes and phases provided using the analytically derived formulae by Montgomery & O'Donoghue (1999). However, it is known that these uncertainties are underestimated because the intrinsic signal in the light curves is superimposed not only by white noise but also by other noise sources (see, for example, Kallinger, Reegen & Weiss 2008). The real scatters in our data should be about twice the formal ones as suggested by earlier authors (Handler et al. 2000; Bruntt et al. 2007).

Fig. 6 shows our investigation on the frequency content at different stages. When eight peaks are removed from the light curves, a few peaks remain in the residuals in the region of the low frequencies (at $f_9 = 1.513$ with A = 1.8 mmag, S/N = 3.8, and $f_{10} = 2.662$ cd^{-1} with A = 1.5 mmag, S/N = 3.3). None of them is significant. However, it is interesting to note that f_{10} could be interpreted as $f_5 - f_1 = 2.661$ cd^{-1}. Fig. 7 shows the light curves of Y Cam (after extracting the binarity) together with the Fourier fitting solution of Table 7. As can be seen, the synthetic light curves satisfactorily fit the observations.

As seen in Table 7, there are two pairs of peaks ($f_2 = 18.31$ cd^{-1} and $f_4 = 19.38$ cd^{-1} or $f_5 = 17.71$ cd^{-1} and $f_8 = 19.70$ cd^{-1}) which could be produced by problems with the daily 1 cd^{-1} alias in our data set. With the aim to gain reliability in our results, we have checked our results by analysing different subset combinations, both with and without the SNO/T90 contribution. The results are consistent with the full solution listed in Table 7 and, in all cases, the two pairs of peaks are found. Thus, it suggests that all the peaks in Table 7 are real, not produced by alias effects.

5.1.2 Close pairs or amplitude variability?

We have also analysed the reliability of the close frequency pair $f_1 = 15.046\,93$ cd^{-1} and $f_3 = 14.988\,33$ cd^{-1} in order to study if this pair really corresponds to two independent peaks, or if it is produced by only one excited mode with changes in amplitude. If real, the light curves produced by the set f_1 and f_3 should show variations in amplitude and phase according to a beating period of $P_{\rm beat} = 17.0648$ d, which corresponds to $f_{\rm beat} = f_1 - f_3 = 0.058\,60$ cd^{-1}. Moreover, these changes in amplitude and phase must vary synchronously with a phase shift close to 90°. However, if the pair of peaks is produced by only one frequency with variable amplitude, then phase variations are not expected.

With this aim, we have followed a procedure similar to that described in Breger & Pamyatnykh (2006) to check our observations with both double- and single-frequency models. First, a double-frequency model was built using the solution provided by our frequency analysis for f_1 and f_3, and listed in Table 7. Thus, the

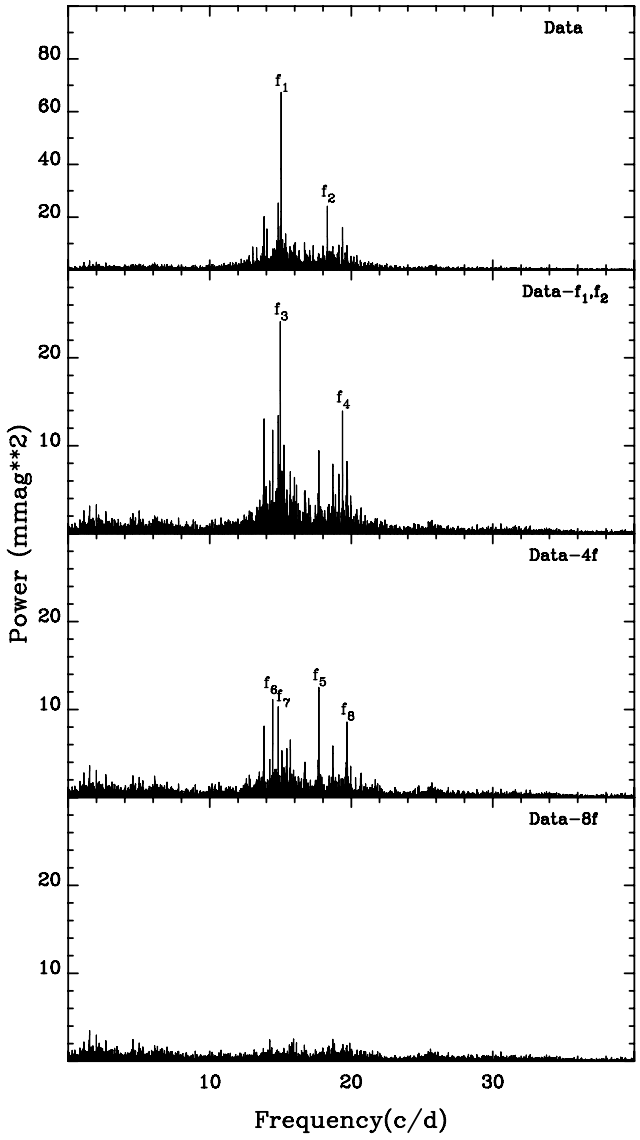

Figure 6. Power spectra of Y Cam before and after removing different sets of simultaneously optimized peaks.

predictions of the synthetic double-frequency light curve over the full range of observations were taken into account and compared with the single-frequency predictions corresponding to the main peak f_1. The results of the two-frequency model are shown as thick dotted lines in Fig. 8.

On the other hand, the observational data were pre-whitened for all the frequencies in Table 7 excluding f_1 and f_3. The data were divided into time bins commonly covering about one or two close observing nights of good quality. The coverage, in each bin, depended on the number and quality of the measurements in order to perform a reliable Fourier fit to the data. In this way, 25 bins were built. Next, assuming f_1 as the best single-frequency solution, the mean amplitudes and phase shifts were calculated for each bin. The results are shown as open circles in Fig. 8, where it is evident that the double-frequency model is responsible for the amplitude and phase variations.

5.1.3 Comparison with older data sets

The set of frequencies listed in Table 7 can be compared with the results found by earlier authors. That is, those found by Kim et al. (2002) (their table 1) for observations collected during the period 2000–2001 or those obtained by Broglia & Conconi (1984) (Group I, collected in 1961–1962, and Group II, collected during the period 1981–1982). Our results are consistent with those found by these authors. In particular, the peaks around f_1, f_2, f_5 and f_7 were already detected by Kim et al. (2002). However, the other four remaining frequencies in our Table 7 were not detected in the work of Kim et al. (2002). This is probably due to their data set not being large enough to resolve the close frequency pairs. Another possibility is the existence of amplitude variability for some modes.

Concerning the amplitudes of the modes, it seems that the present amplitudes (see Table 8 and filter *y*) are consistent with those determined by Kim et al. (2002) or by Broglia & Conconi (1984). Note that the amplitudes listed in table 1 of Kim et al. (2002) for the Broglia & Conconi's (1984) results are peak-to-peak amplitudes.

5.2 Multicolour photometry

Table 8 lists the results of the Fourier fit when the solution of eight frequencies in Table 7 is applied to the multicolour *uvby* photometry collected at SNO. As seen, the results are consistent with each other within the present uncertainties. Only in the *u* filter, some of the frequencies seem to be not significant. This is because of the much higher noise level in this filter. Moreover, the amplitudes of the peaks are not exactly in the same order as in Table 7. In particular, the relative amplitude of f_4 is much smaller than expected from Table 7. This is due to simultaneously fitting the eight-frequency solution, with various close frequency pairs, to only the SNO/T90 contribution which is much smaller than the full data set (it is only about 30 per cent of the total data set). Fig. 9 shows the observed light curves and predictions for orbital phases around the primary eclipses, for data points from the SNO/T90 contribution in the Strömgren *v* filter. Table 9 lists the observed phase shifts and amplitude ratios determined for the most significant frequencies in Table 8. Preliminary insights on the radial and/or non-radial nature of the excited modes can be performed by checking our values in Table 9, with the work of Garrido, García-Lobo & Rodríguez (1990). This suggests that most frequencies probably correspond to non-radial modes.

5.2.1 Mode identification

Mode identification, i.e. determination of the radial order, n, the spherical harmonic degree, ℓ, and azimuthal order, m, of a given pulsational frequency, is a prerequisite for asteroseismic studies. The radial order can be determined from the pulsation frequencies and the mean density of the star. Pulsation constants calculated for the $f_1 - f_8$ frequencies are given in the last column of Table 7. The estimated error bars are of $\sim$12 per cent taking into account the parameters in Table 5.

To get information on the angular numbers, ℓ and m, we have to employ additional observables. A possibility is offered by the fact that the light and line profile variations of pulsating stars depend on the mode geometry. The most widely applied method makes use of amplitudes and phases from multi-passband photometry.

There are two methods of photometric mode identification. The first approach is based on the amplitude ratios and phase differences in various passbands, and requires input from atmospheric

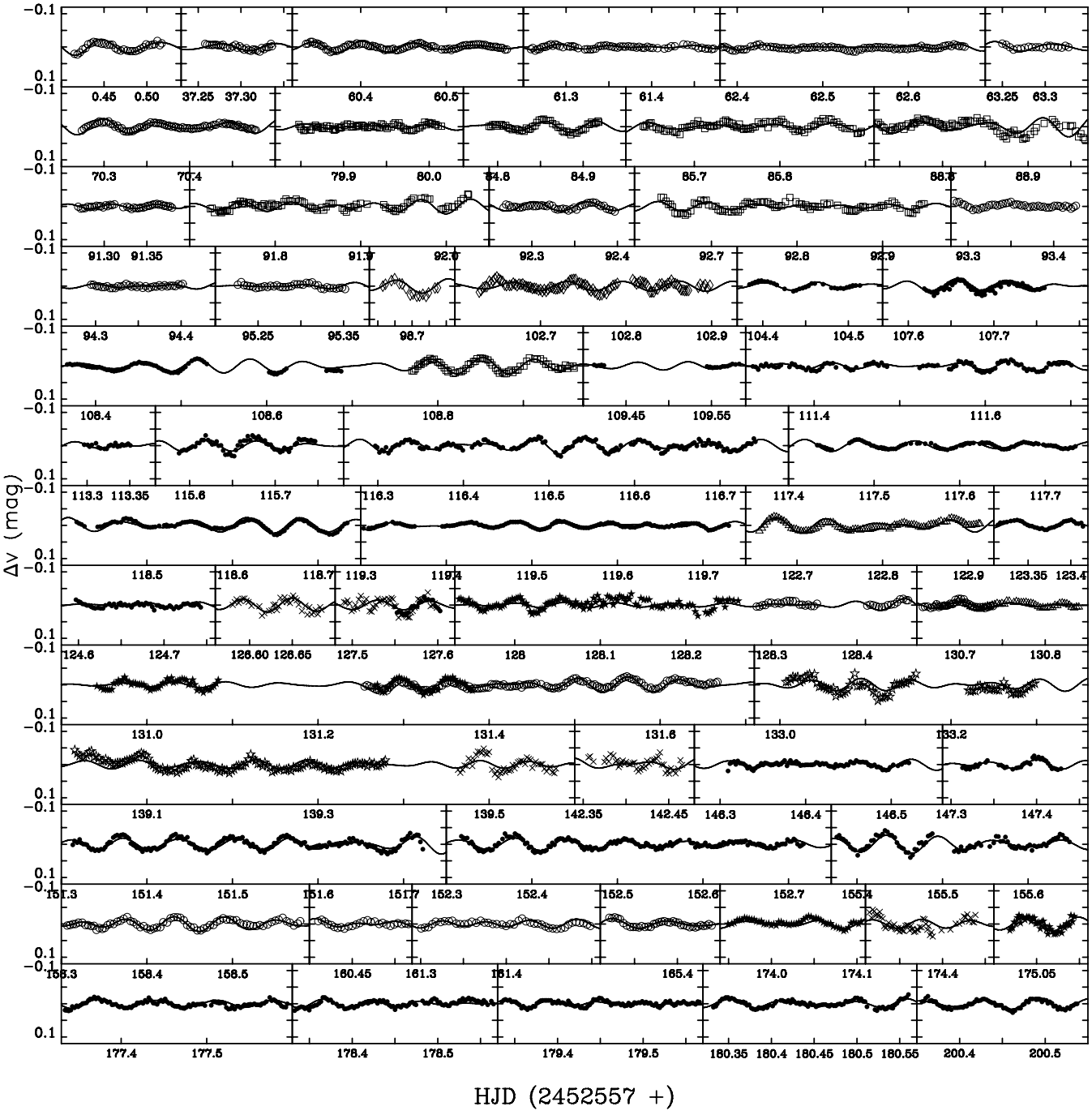

Figure 7. Light curves of Y Cam corresponding to the out-of-eclipse residuals after removing the binary curve and Fourier fitting using the eight-frequency solution of Table 7. The different contributions are: SNO (filled circles), BHO (open circles), CNAO (crosses), SOAO (filled stars), BAO (open stars), KPNO (open triangles), OPO (open diamonds) and MLO (open squares).

models as well as from non-adiabatic pulsational theory (Cugier, Dziembowski & Pamyatnykh 1994; Balona & Evers 1999; Garrido 2000). If effects of rotation can be neglected then the photometric amplitude ratios and phase differences are independent of the inclination angle, i, azimuthal order, m, and the intrinsic amplitude of the radius variations, ε. The second version utilizes amplitudes and phases themselves and needs just the input from models of stellar atmospheres (Daszyńska-Daszkiewicz, Dziembowski & Pamyatnykh 2003; Daszyńska-Daszkiewicz et al. 2005a; Daszyńska-Daszkiewicz, Dziembowski & Pamyatnykh 2005b). This is because the ℓ degree and the complex non-adiabatic parameter f, which describes the ratio of the bolometric flux variation, are determined simultaneously from observations.

We applied both versions of photometric methods to determine the ℓ values of pulsational modes observed in the primary component of Y Cam. The results of the first one are shown in Fig. 10. On the left-hand side, we have plotted the amplitude ratios in the (v, y) passbands as a function of the corresponding phase shifts. A very

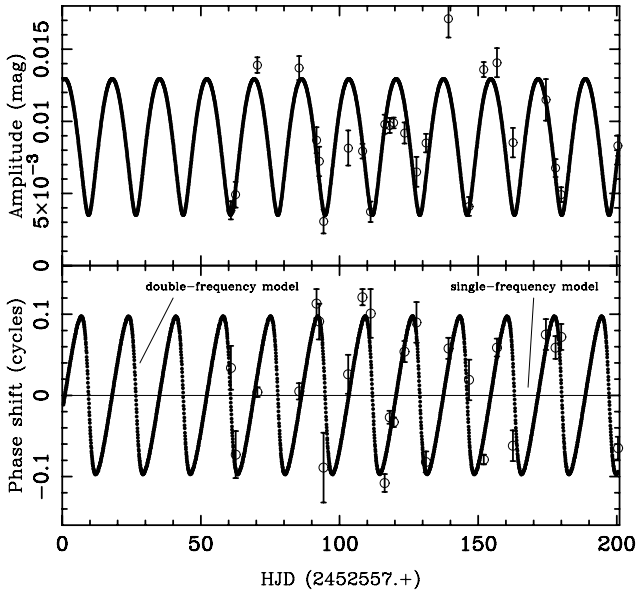

Figure 8. Amplitude and phase variations of the frequency $f_1 = 15.046\,93$ cd^{-1} over the full observing run. Phase variations are given in cycles. The open circles represent the observations, while the thick dotted lines represent the predictions by the two-frequency model of f_1 and f_3 as two independent frequencies with constant amplitude. This diagram shows a very good agreement between them. The variations are according to a beating period of $P_{\rm beat} = 17.0648$ d. The single-frequency model with variable amplitude (thin line) excludes changes in phase.

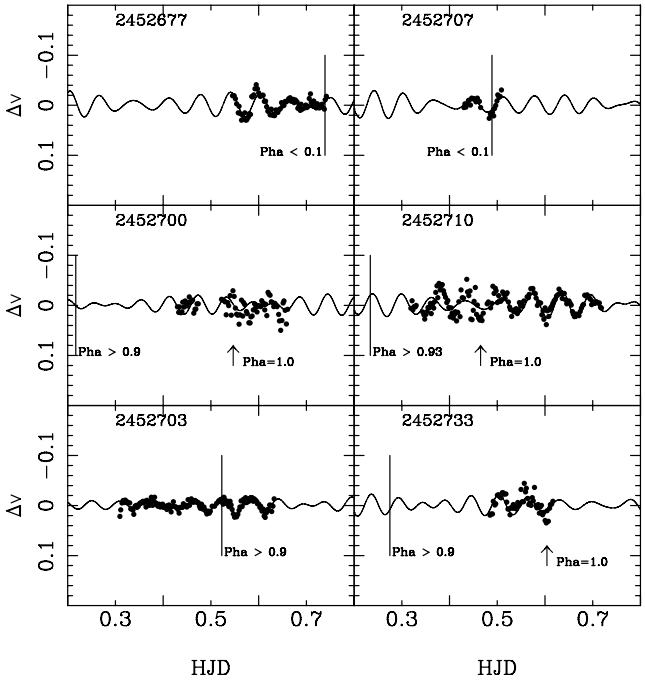

Figure 9. Observed light curves and predictions for orbital phases around the primary eclipse and SNO/T90 data set in filter v.

similar diagram is found for the pairs (b, y). On the right-hand panel, the diagram for the (u, y) pairs is shown. We considered modes up to $\ell = 4$ because the higher ℓ modes suffer strong averaging effects. The theoretical values were computed for the stellar parameters of mass, effective temperature and luminosity in agreement with those found in previous sections for the primary component of the system, assuming $X = 0.70, Z = 0.02$, the MLT convective parameter $\alpha_{\rm conv} = 0$, the OP opacities and the solar composition by Asplund et al. (2005). We included only unstable modes in the frequency range of 13–20 cd^{-1} which corresponds to the observed frequency range of Y Cam. Here, we rely on the Vienna atmosphere models and pulsational inputs obtained by means of the Dziembowski's code (Dziembowski 1977).

In Fig. 11 we can see the results from the method by Daszyńska-Daszkiewicz et al. (2003, 2005a,b). The value of χ^2 was computed for the same stellar model except that three values of effective temperature were considered. As before, the Vienna atmosphere models were used. The χ^2 is a measure of the fit between the observed amplitudes and phases and the theoretical ones in all passbands. This method is independent of uncertainties of pulsational computation,

Table 8. Fourier fit applied to the four *uvby* filters and SNO data set. Standard deviations of the residuals are 20.6 (u), 7.0 (v), 6.4 (b) and 8.1 (y) mmag.

	u			*v*			*b*			*y*		
Frequency	A (mmag)	φ (rad)	S/N	A (mmag)	φ (rad)	S/N	A (mmag)	φ (rad)	S/N	A (mmag)	φ (rad)	S/N
	±0.80			±0.28			±0.25			±0.32		
f_1	8.70	3.219	6.7	9.48	3.020	14.8	8.00	3.079	14.5	5.93	3.192	11.0
		94			29			32			54	
f_2	5.58	2.596	4.3	6.10	2.604	10.7	5.55	2.628	10.5	4.52	2.729	8.5
		143			44			44			69	
f_3	4.76	2.141	3.7	5.49	1.545	8.6	4.62	1.662	8.4	3.70	1.834	6.9
		179			53			57			91	
f_4	3.37	1.015	2.6	2.72	0.739	4.8	2.64	0.741	5.0	2.23	0.776	4.2
		233			98			92			138	
f_5	3.99	0.761	3.1	4.42	0.786	7.8	3.30	0.848	6.2	2.73	1.038	5.2
		208			64			78			120	
f_6	4.55	0.923	3.5	3.83	0.780	6.0	3.42	0.650	6.2	2.52	0.555	4.7
		175			71			72			124	
f_7	1.93	3.166	1.5	2.97	3.260	4.6	2.60	3.281	4.7	2.90	3.152	5.4
		468			104			107			123	
f_8	2.62	1.867	2.0	2.70	2.039	4.7	2.55	1.859	4.8	1.96	1.700	3.7
		307			101			97			161	

Table 9. Observed phase shifts and amplitude ratios.

Freq	$\varphi_u - \varphi_y$ (°)	$\varphi_v - \varphi_y$ (°)	$\varphi_b - \varphi_y$ (°)	A_u/A_y	A_v/A_y	A_b/A_y
f_1	1.5	−9.9	−6.5	1.47	1.60	1.35
	8.5	4.8	4.9	16	10	8
f_2	−7.6	−7.2	−5.8	1.23	1.35	1.23
	12.2	6.5	6.5	20	11	10
f_3	17.6	−16.6	−9.9	1.29	1.48	1.25
	15.4	8.2	8.5	24	15	13
f_5	−15.9	−14.4	−10.9	1.46	1.62	1.21
	18.8	10.6	11.4	34	22	17
f_6	21.1	12.9	5.4	1.81	1.52	1.36
	17.2	11.2	11.3	39	22	20

e.g. connected with the treatment of convective transport in the outer layers of δ Sct stars. On the other hand, comparison of empirical and theoretical values of the f-parameter can yield stringent constraints on various parameters of marco- and microphysics, e.g. convection, opacities (Daszyńska-Daszkiewicz et al. 2003, 2005a,b).

As we can see, the identification of ℓ from both approaches is ambiguous for most observed frequencies in Y Cam (see Figs 10 and 11). Nevertheless, a tentative identification of ℓ can be given as inferred from Fig. 11: f_1: $\ell = 3$; f_2: $\ell \leq 3$; f_3: $\ell = 2, 3$; f_4: $\ell \leq 3$; f_5: $\ell \leq 3$; f_6: $\ell \leq 3$; f_7: $\ell = 4$; f_8: $\ell = 3$. The results for the three first periodicities (f_1,f_2 and f_3) are the most consistent ones with those suggested from Fig. 10.

6 DISCUSSION

6.1 Mode spacings

The schematics of the oscillation spectrum for the pulsating component of Y Cam are shown in Fig. 12. The spectrum shows the regular frequency spacings. The frequencies pairs f_5, f_6 and f_2, f_1 are spaced by 3.2608 ± 0.000 34 and 3.2652± 0.000 18 cd^{-1}, respectively. Frequencies f_4 and f_5 are spaced by 1.6729 ± 0.000 31 cd^{-1} (19.3619 μHz) – very close to the value of the half-spacing of f_5,f_6 and f_2,f_1. Such regular spacing of the low overtone (n<6) modes resembles that of δ Sct star XX Pyx (Handler et al. 1997, 2000) and of the λ Boo-type star 29 Cyg (Mkrtichian et al. 2007b). The regular frequency spacings are inherent in the p-mode spectra of some types of pulsating main sequence (e.g. solar type, roAp stars) and F and K giant stars and caused by consecutive overtones.

If we assume that the frequency spacing of 3.26 cd^{-1} (37.73 μHz) is the spacing between consecutive overtones of the modes belonging to the same degree of l, then half of this spacing for frequencies f_4 and f_5 is expected to be the spacing between modes of even and odd l-values.

The expected general spacings of the consecutive (high-order) overtones $\Delta\nu$ in Y Cam can be calculated using the following calibration:

$$\Delta\nu = 135 M/\mathrm{M}_\odot^{0.5} R/R_\odot^{-1.5}\ \mu\mathrm{Hz}. \quad (1)$$

Substitution of the mass and the radius (and their formal errors) from Table 5 results in $\Delta\nu = 34.7 \pm 4.3$ μHz – that is nearly close to spacings 37.73 μHz found from the observed oscillation spectrum.

Close matching of the expected and observed values confirms that the frequencies are most likely the consecutive overtones. Interpretation of the halves of spacings formed by pairs f_5 with f_4 and f_2 with f_8 as the spacings of modes of odd and even l-values, respectively, could be accepted with some care.

Assuming the synchronization of components, and having the Y Cam system for an orbital period of $P_{\rm orb} = 3.3057$ d, we can expect about $m \times \Omega$ magnitude of rotational splitting of modes in the observer's coordinate frame due to Doppler effect, where $\Omega = 1/P_{\rm orb} = 0.3025$ cd^{-1} (3.501 μHz) (m is the azimuthal order of non-radial mode).

For $|m| \geq 2$, splitting is comparable with small-frequency separations of pairs of modes with the equal l-oddity (namely, $\ell = 0, 2, \ldots$ or $\ell = 1, 3, \ldots$), thus mode identification can be

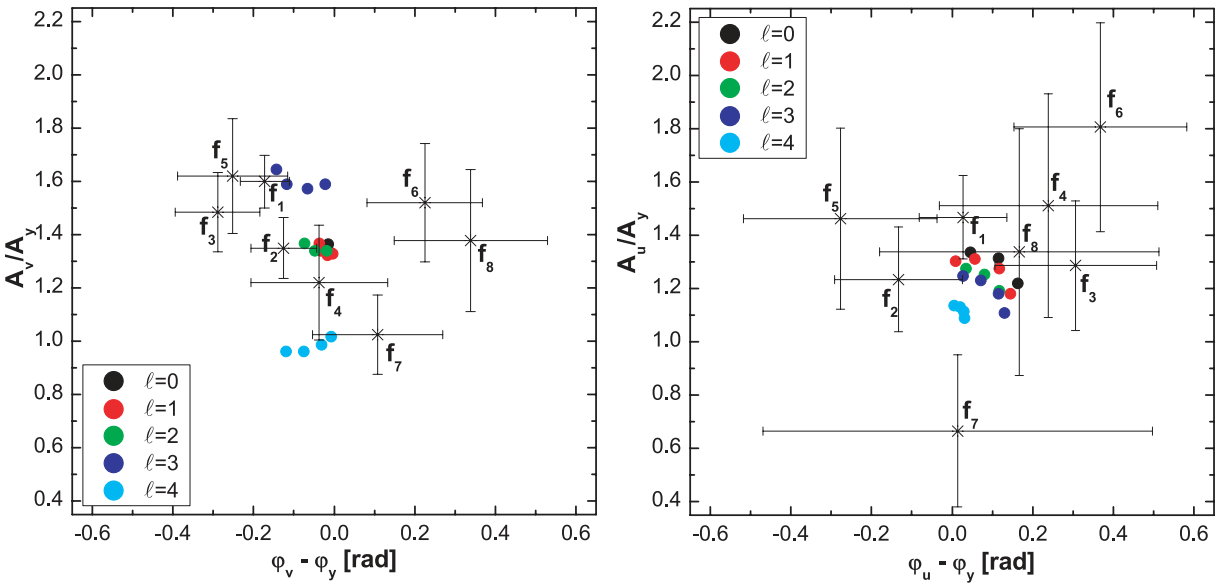

Figure 10. Location of modes observed in the pulsational light curves of Y Cam on the photometric diagnostic diagrams. Theoretical values were computed for $M = 1.67\,\mathrm{M}_\odot$, $\log T_{\rm eff} = 3.876$ and $\log L/\mathrm{L}_\odot = 1.39$ assuming $X = 0.70, Z = 0.02$ and $\alpha_{\rm conv} = 0$. We considered only unstable modes in the frequency range of 13–20 cd^{-1}, and the spherical harmonic degrees, ℓ, up to 4.

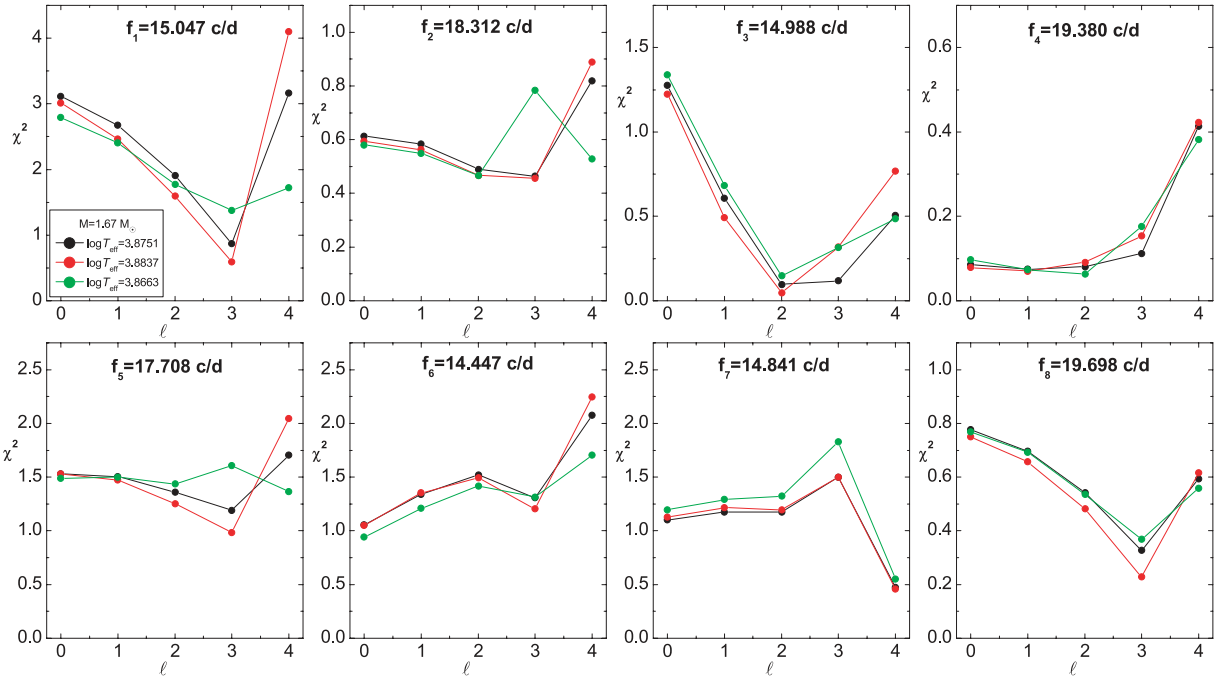

Figure 11. Values of the discriminant χ^2 as a function of the ℓ degree for the eight oscillation frequencies observed in Y Cam. The adopted stellar parameters are the same as in Fig. 10 and three different values of $\log T_{\rm eff}$ were considered.

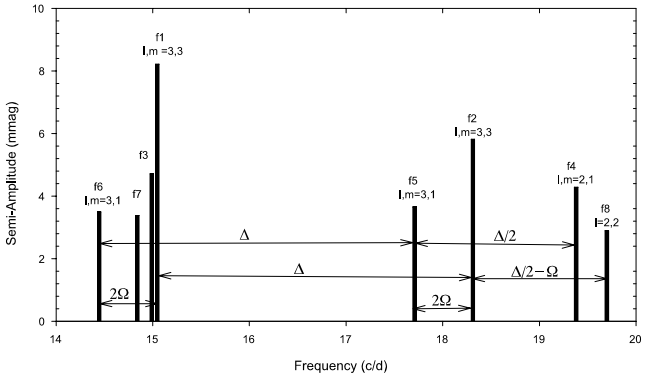

Figure 12. Schematic frequency spectrum and spacings of Y Cam. Mode identifications are tentative (see text).

complicated if based only on observed, probably mixed, frequency spacings.

For example, the observed spacing of f_8 and f_2 is 1.3855 cd^{-1} (16.0359 μHz), which is exactly equal to $\Delta/2 - m\Omega$ for the case of $m = 1$. Other examples are spacings of f_1 and f_6 that are exactly $f_1 - f_6 = 2\Omega$ and $f_2 - f_5 = 2\Omega$ too. This means an m difference of 2. Such exact spacing of the values of multiplets of orbital/rotation period is indicating the complex nature of oscillation spectrum consisting of modes of different m values.

Moreover, we also note that the exact equality of spacings for f_5,f_6 and f_2,f_1 pairs suggests that these consecutive overtones in modal pairs have the same m-orders, i.e. they belong to consecutive overtones of the same l, m pairs. Some tentative results are shown in Fig. 12.

6.2 Mode visibility

In the case of the dominant mode, f_1, we have obtained the degree $\ell = 3$ as the most reliable and this identification seems to be unique. Let us discuss this result regarding the mode visibility. If we assume that the inclination angle of Y Cam is the same as the orbital one as derived from the WD solution, $i = 85^\circ$ (Table 4), then we can safely exclude modes with the nodal line on the equator. It means that only the even-parity modes can be considered, i.e. modes with $\ell - |m| = 2j$, where $j = 0, 1, 2, \ldots$ Thus, in the case of $\ell = 3$ we can take only $|m| = 1$ or $|m| = 3$. The other effect which has to be taken into account is a strong averaging of pulsational modes with $\ell > 2$ (Daszyńska-Daszkiewicz et al. 2002). Assuming the same intrinsic amplitude for all modes, $\varepsilon = 0.005$, the inclination angle $i = 85^\circ$ and excluding the odd-parity modes, we estimated the y amplitudes of the $\ell = 3$ modes about one order of magnitude lower than those of the radial or dipole modes.

Thus, how probable is the $\ell = 3$ mode for the dominant frequency of Y Cam? We have two explanations of this identification. First, the intrinsic mode amplitude of $\ell = 3$ can be larger than those of the lower ℓ modes. Unfortunately, we are not able to check this argument as the mechanism of the mode selection is not known yet. Secondly, the values of photometric amplitudes of the Y Cam frequencies are comparable to each other. Looking at the observed oscillation spectrum, we can see that there is no peak sticking out of others as in the case of many δ Sct stars, e.g. FG Vir (Breger et al. 2005). Moreover, also for the remaining frequency peaks there is an indication for the harmonic degrees $l > 2$.

Consequently, we can assume that the most probable identification of the angular number for the dominant frequency of Y Cam is $\ell = 3$ with $|m| = 1$ or 3. Then two identifications permitted by mode visibility are $l, m, n = 3, \pm 3, n$ or $3, \pm 1, n$ for f_1 and $l, m, n + 1 = 3, \pm 3, n + 1$ or $3, \pm 1, n + 1$ for f_2, respectively. We

think that the first one is reliable for f_1 while the second identification is probably occupied by the f_6 mode.

The mode identification for f_6 from multicolour photometry is $l \leq 3$. If the frequencies f_5 and f_6, that are spaced from respectively f_2 and f_1 on exactly $-2 \times \Omega$, are shifted due to Doppler effect, then identification, among permitted by mode visibility, is for f_6: l, m, $n = 3, 1, n$ while for f_5: l, m, $n = 3, 1, n + 1$.

The l, m identification of other modes is ambiguous. For modes f_4 and f_8 nearly half-spaced from f_5 and f_2 and spaced between each other on Ω, we can suggest that (i) they belongs to modes with opposite ℓ-oddity to f_2 and f_5 modes – i.e. $\ell = 2$ or $\ell = 0$ radial modes; (ii) the m order of f_8 is larger on $\delta m = 1$ than the azimuthal quantum number of f_4 mode. That satisfy the case of l, $m = 2, 1$ identification for f_4 and l, $m = 2, 2$ identification for f_8. The identification for f_4 mode does not fit well the visibility criteria, otherwise we have to assume vary large intrinsic amplitude of this mode.

7 CONCLUSIONS

Based on the data of a three-continent multisite photometric campaign on the Algol-type eclipsing binary system Y Cam, we derive improved component properties and detect a rich oscillation spectrum for the δ Sct-type pulsating component of this system, consisting of eight oscillation modes in a well-defined region of the frequency domain. Our results confirm the frequencies already detected by earlier authors with some additional significant peaks. The observed amplitudes are also consistent with those derived from older data sets. Moreover, f_1 and f_3 form a frequency doublet with a beat period of $P_{\rm beat} = 17.065$ d.

The collected multicolour photometry is used to perform an ℓ identification of the excited modes. The oscillation spectrum of Y Cam shows the regular general spacings by $\Delta = 3.26$ cd^{-1} (37.73 μHz) and by $\Delta/2$ indicating the excitation of consecutive overtones of odd and even l-degree modes.

A tentative cross-identification is provided for most of the detected excited modes on the basis of the collected multicolour photometry, the observed frequency spacings and restrictions implied by the mode visibility in the case of the on-equator visible pulsating component of the Y Cam system. Certainly, direct comparison between observed and theoretical frequencies calculated from pulsation models of Y Cam with accurate stellar parameters derived from binarity should be the best way for reliable mode identifications. This much more detailed work is out of the scope of the current paper.

ACKNOWLEDGMENTS

This research was partially supported by the Junta de Andalucía and the Dirección General de Investigación (DGI) under project AYA2009-10394 and ESP2004-03855-C03-01. ER acknowledges Gerald Handler's effort in collecting additional data using the 75-cm Vienna APT. This work made use of the Simbad data base, operated at CDS, Strasbourg, France. Part of the data was acquired with equipment purchased thanks to a research fund financed by the Belgian National Lottery (1999). Support from the Fund for Scientific Research – Flanders (Belgium) through project G.0332.06 (TBC) is also acknowledged. DEM acknowledges that his work was done as a part of research activity of the Astrophysical Research Center for the Structure and Evolution of the Cosmos (ARCSEC) which is supported by the Korean Science and Engineering Foundation.

REFERENCES

Asplund M., Grevesse N., Sauval A. J., Allende Prieto C., Blomme R., 2005, A&A, 431, 693
Baker E. A., 1937, MNRAS, 98, 65
Balona L. A., Evers E. A., 1999, MNRAS, 302, 349
Batten A. H., Fletcher J. M., MacCarthy D. G., 1989, Publ. Dom. Astrophys. Obs., 17
Breger M., 1979, PASP, 91, 5
Breger M., Pamyatnykh A. A., 2006, MNRAS, 368, 571
Breger M. et al., 1993, A&A, 271, 482
Breger M. et al., 1999, A&A, 349, 225
Breger M. et al., 2005, A&A, 435, 955
Broglia P., 1973, Inf. Bull. Var. Stars, 823, 1
Broglia P., Conconi P., 1984, A&A, 34, 89
Broglia P., Marin F., 1974, A&A, 34, 89
Bruntt H. et al., 2007, MNRAS, 378, 1371
Christiansen J. L., Derekas A., Ashley M. C. B., Webb J. K., Hidas M. G., Hamacher D. W., Kiss L. L., 2007, MNRAS, 382, 239
Cugier H., Dziembowski W. A., Pamyatnykh A. A., 1994, A&A, 291, 143
Daszyńska-Daszkiewicz J., Dziembowski W. A., Pamyatnykh A. A., Goupil M.-J., 2002, A&A, 392, 151
Daszyńska-Daszkiewicz J., Dziembowski W. A., Pamyatnykh A. A., 2003, A&A, 407, 999
Daszyńska-Daszkiewicz J., Dziembowski W. A., Pamyatnykh A. A., Breger M., Zima W., Houdek G., 2005a, A&A, 438, 653
Daszyńska-Daszkiewicz J., Dziembowski W. A., Pamyatnykh A. A., 2005b, A&A, 441, 641
Díaz-Cordovés J., Claret A., Giménez A., 1995, A&AS, 110, 329
Dziembowski W. A., 1977, Acta Astron., 27, 95
Gamarova A. Y., Mkrtichian D. E., Rodríguez E., Costa V., López-González M. J., 2003, PASP, 292, 369
Garrido R., 2000, PASP, 210, 67
Garrido R., García-Lobo E., Rodríguez E., 1990, A&A, 234, 262
Handler G., Shobbrook R. R., 2002, MNRAS, 333, 251
Handler G. et al., 1997, MNRAS, 286, 303
Handler G. et al., 2000, MNRAS, 318, 511
Hauck B., Mermilliod M., 1998, A&AS, 129, 431
Ibanoglu C., Tas G., Sipahi E., Evren S., 2007, MNRAS, 376, 573
Jeon Y. B., Kim S.-L., Lee M. G., Lee H., Lee J. W., 2006, ApJ, 636, L129
Kallinger T., Reegen P., Weiss W. W., 2008, A&A, 481, 571
Kim S.-L., Lee J. W., Youn J.-H., Kwon S.-G., Kim C., 2002, A&A, 391, 213
Kim S.-L., Lee J. W., Kwon S.-G., Youn J.-H., Mkrtichian D. E., Kim C., 2003, A&A, 405, 231
Kim S.-L., Lee C. U., Lee J. W., 2006, Mem. Soc. Astron. Ital., 77, 184
Kim S.-L., Lee C. U., Lee J. W., Youn J.-H., 2007, Comm. Asteroseismol., 150, 68
Lampens P. et al., 2008, Comm. Asteroseismol., 153, 54
Lampens P. et al., 2010, A&A, submitted
Lee J. W., Kim C. H., Kim S.-L., Youn J.-H., Kwon S.-G., 2002, J. Astron. Space Sci., 19, 187
Lehmann H., Mkrtichian D. E., 2004, A&A, 413, 393
Lehmann H., Mkrtichian D. E., 2008, A&A, 480, 247
Lenz P., Breger M., 2005, Comm. Asteroseismol., 146, 5
Mezzetti M., Cester B., Giuricin G., Mardirossian F., 1980, A&AS, 39, 265
Mkrtichian D. E. et al., 2004, A&A, 419, 1015
Mkrtichian D. E. et al., 2007a, PASPC, 370, 194
Mkrtichian D. E. et al., 2007b, AJ, 134, 1713
Montgomery M. H., O'Donoghue D., 1999, Delta Scuti Star Newsletter, 13, 28
Moon T. T., Dworetsky M. M., 1985, MNRAS, 217, 305
Mossakovskaya L., 1993, Inf. Bull. Var. Stars, 3902
Rodríguez E., Breger M., 2001, A&A, 366, 178
Rodríguez E., López de Coca P., Rolland A., Garrido R., 1990, Rev. Mex. Astron. Astrofís., 20, 37

Rodríguez E., Rolland A., López-González M. J., Costa V., 1998, A&A, 338, 905
Rodríguez E., López-González M. J., Rolland A., Costa V., González-Bedolla S. F., 2001, A&A, 376, 489
Rodríguez E., Costa V., Handler G., García J. M., 2003, A&A, 399, 253
Rodríguez E. et al., 2004a, MNRAS, 347, 1317
Rodríguez E. et al., 2004b, MNRAS, 353, 310
Soydugan E., Soydugan F., Demircan O., Ibanoglu C., 2006, MNRAS, 370, 2013
Struve O., Horak H. G., Canavaggia R., Kourganoff V., Colacevich A., 1950, ApJ, 111, 658
van Hamme W., Wilson R. E., 2003, PASP, 298, 323
Wilson R. E., 1979, ApJ, 234, 1054
Wilson R. E., 1990, ApJ, 356, 613
Wilson R. E., Devinney E. J., 1971, ApJ, 166, 605
Wilson R. E., van Hamme W., 2004, 'Computing Binary Star Observables', Introduction to the Wilson–Devinney programme

This paper has been typeset from a TEX/LATEX file prepared by the author.